JOURNAL OF MATERIALS SCIENCE 31 (1996) 3349–3359

Fragmentation in alumina fibre reinforced epoxy model composites monitored using fluorescence spectroscopy

R. B. YALLEE, M. C. ANDREWS, R. J. YOUNG
Manchester Materials Science Centre, UMIST/University of Manchester, Grosvenor Street, Manchester M1 7HS, UK

It has been found that well-defined fluorescence R_1 and R_2 lines can be obtained from PRD-166 alumina–zirconia fibres and that the fluorescence R lines shift with applied stress. They are found to shift to higher wavenumber when subjected to tensile deformation and to lower wavenumber in compression. The stress-sensitive fluorescence R_2 line has been used to map the distribution of stress along PRD-166 fibres embedded in an epoxy resin matrix cured under different conditions. It has been shown that the distributions of stress along the PRD-166 fibres at different levels of matrix strain are consistent with those predicted by conventional shear–lag analysis. The interfacial shear stress has been derived from the point-to-point variation of stress along the fibre. The fluorescence technique has also been used to map the stress distribution along a PRD-166 fragment in an epoxy matrix during a single-fibre fragmentation test where it is found that debonded regions propagate along the fibre fragments during loading, after initial fragmentation has occurred.

1. Introduction

The distributions of stress and strain along a discontinuous fibre in a matrix have been analysed by theoretical modelling [1–3] over the past forty years. Cox [1] gave the first solution for fibre stress distribution along a fibre/matrix interface with both the fibre and matrix undergoing elastic deformation. The distribution of stress along a fibre with a debonded region near the fibre ends and perfect adhesion in the central region of the fibre was presented by Piggott [2]. Kelly and Tyson [3] presented an analysis for the distribution of stress along a fibre in the case of an elastic fibre in a plastic matrix.

Over the past decade, the distributions of stress and strain along a variety of types of fibre in different matrices has been determined experimentally using the technique of Raman spectroscopy [4–7]. This technique is based on the observation that the characteristic Raman bands obtained from the fibres shift upon the application of stress. The approximately linear stress- or strain-dependent shift of the Raman bands obtained from a fibre in air is then used to relate the Raman band shifts, obtained from a fibre in a deformed transparent matrix, to the point-to-point variation of stress or strain in that fibre.

Recently, well-defined fluorescence R lines have been obtained from PRD-166 alumina–zirconia fibres in this laboratory using an unmodified Raman microprobe system [8]. The characteristic fluorescence R lines are due to the presence of chromium impurities in the alumina crystals of the fibres [9]. The same fluorescence phenomenon has also been observed from ruby [9], sapphire [10] and single crystal alumina fibres [11–13]. The fluorescence R lines from the alumina-based materials [9–12] have been found to shift approximately linearly with the application of stress. A linear dependence of fluorescence R lines with strain has also been observed for PRD-166 alumina–zirconia fibres [8]. The stress- or strain-sensitive fluorescence R lines from the PRD-166 fibre raise the possibility of determining the strain distribution along a PRD-166 fibre in a matrix, in an analogous way to the determination of fibre strain using the Raman phenomenon [4–7].

In this work, the dependencies of the wavenumbers of fluorescence R lines from PRD-166 fibres upon applied tensile and compressive strain and tensile stress are determined. This dependence is then used to map the distribution of axial fibre stress along a PRD-166 fibre, embedded fully in an epoxy matrix, undergoing fragmentation caused by an applied matrix tensile stress. The fibre stress distribution is then used to generate the interfacial shear stress distribution along the fragments. The residual thermal stresses in PRD-166 fibres in a hot-cured epoxy matrix are also compared with those expected from theoretical analysis.

2. Experimental procedure

2.1. Fibres and single-fibre composites

The PRD-166 fibres used in this work have a mean diameter of 18.8 $\pm$ 0.6 μm. They were from the same

0022–2461 © *1996 Chapman & Hall*

two used for the systematic study of the relationship between structure and properties described elsewhere [14].

The single-fibre composites were prepared using a two-part epoxy resin consisting of 100 parts by weight of Araldite LY5052 resin to 38 parts by weight of HY5052 hardener. A square "picture frame" mould was filled with half of the resin/hardener mixture and this was allowed to cure partially before a few short PRD-166 fibres and the rest of the mixture were added. After curing at room temperature (22 ± 2 °C) for seven days, the resin composite was cut into strips which were subsequently polished to 3 mm thickness and shaped into dumb-bell specimens, ensuring that a PRD-166 fibre was located in the centre of the test region. "Hot-cured" single-fibre composites were also prepared from resin composites which were cured at room temperature for 24 h and then post-cured at 80 °C for 8 h. The room temperature cured epoxy matrix has a tensile modulus and shear yield stress of about 3.0 GPa and 43 MPa respectively [15]. The hot-cured epoxy resin had a tensile modulus of 3.0 GPa and a yield stress of 45 MPa [16].

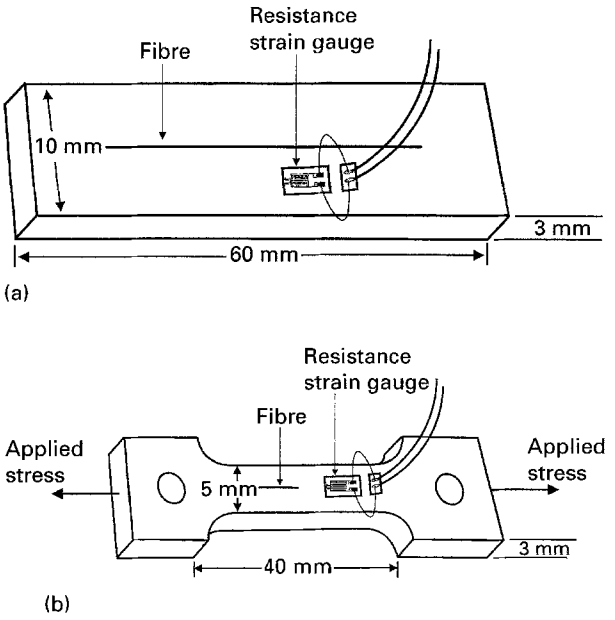

Figure 1 Schematic diagram of (a) four-point bending specimen, (b) model single-fibre composite.

2.2. Fluorescence spectroscopy

Fluorescence spectra were obtained from PRD-166 fibres and single-fibre composites during deformation using an unmodified Raman microprobe system [8]. It is based upon a Spex 1403 double monochromator connected to a modified Nikon optical microscope. The fluorescence spectra were obtained using the 632.8 nm red line of a 15 mW He–Ne laser with an intensity of about 1.0 mW at the fibre surface. This level of laser beam intensity was found to cause minimal shift in the wavenumbers of the fluorescence lines due to heating effects [17]. All measurements were made using a ×40 microscope objective lens with a numerical aperture of 0.65, giving an approximate beam diameter on the specimen of 3 μm. The laser beam was polarised parallel to the fibre axis for all measurements. The beam could be focused on the fibre through several mm of resin within the single-fibre composites and this enabled the deformation of fibres to be monitored directly within the composites.

2.2.1. Fibre straining

Spectra (using ~2 s exposure time) were obtained from fibres, bonded onto poly(methyl methacrylate) (PMMA) strips (3 × 10 × 60 mm) by a thin layer of PMMA, during deformation in a small four-point bending rig which fitted directly onto the microscope stage. The surface strain (≡ the fibre strain) was measured using a resistance strain gauge, of gauge factor 2.09, bonded to the surface of the sample as shown in Fig. 1(a). The strain was increased in steps of about 0.01% for both compressive and tensile deformation. Spectra were also obtained from fibres during deformation in air in a small micrometer-driven straining rig, using 20 and 50 mm gauge lengths, as described in an earlier publication [14]. The strain sensitivity of the fluorescence R lines obtained using the two methods and different gauge length could then be compared.

2.2.2. Fibre stressing

The dependence of the fluorescence band positions upon stress was also determined. This was undertaken using a specially-constructed straining rig, employing a 1 N load cell, which fitted directly upon the microscope stage of the spectrometer. Individual single fibres were fixed to window cards using aluminium foil tabs with cyanoacrylate adhesive and the cards fixed to the straining rig. The edges of the cards were cut, and the stress increased until fibre failure occurred. Spectra were obtained at different levels of applied stress and the positions of the fluorescence bands were determined as a function of the applied axial fibre stress.

2.2.3. Single-fibre composites

The single-fibre composite samples were mounted individually on a Minimat straining rig which was placed on the microscope stage of the Nikon optical microscope. The strain in the matrix was also measured using a resistance strain gauge (Fig. 1(b)). Spectra were recorded along the length of a fibre in a composite specimen (using 5–10 s exposure time) at various levels of tensile matrix strain, up to matrix fracture.

3. Results and discussion

3.1. Deformation of single fibres

The PRD-166 fibres were deformed in both the four-point bending and the micrometer-controlled straining rig. The former rig enables both tensile and compressive deformation to be applied to the fibres whereas only tensile deformation can be applied to the fibres

using the micrometer straining rig. The deformation of the fibres was followed using fluorescence spectroscopy. Fig. 2 shows the fluorescence R lines obtained from a PRD-166 fibre bonded onto a PMMA strip in the undeformed state, subjected to compression (negative) and under tensile (positive) deformation. It can be seen that the peak positions of fluorescence R lines are sensitive to the level of applied strain shifting to higher wavenumber in tension and lower wavenumber in compression. It was found that the peak positions of the fluorescence R lines obtained from the bonded fibres prior to loading were the same (within experimental error) as those obtained from stress-free fibres in air. Thus, negligible residual stresses are induced in the fibre as a result of film shrinkage and/or handling.

The variation of fluorescence wavenumber with applied strain for the R_1 and R_2 lines is shown in Fig. 3(a) and (b), respectively. It can be seen that fluorescence R lines shift to lower and higher wavenumber with increasing compressive and tensile strain respectively, until fibre or film failure occurs as indicated by the arrows. It is clear that the deformation distorts the alumina crystal lattice and alters the energy of the transition between the electronic states and consequently leads to the shift in the wavenumber of the fluorescence R lines [8, 9]. It should be noted that PRD-166 fibres are polycrystalline [14] and so the individual crystal grains in the fibre might be in different states of stress at a given level of applied load. The measured R line shifts will then be an average of the shifts from all crystal grains within the volume of fibre probed by the laser spot.

It can be seen from Fig. 3(a) and (b) that the failure strain of the alumina fibres in compression is considerably higher than that of the fibres in tension. This should be contrasted with the behaviour of aramid [18] and carbon fibres [19] which have relatively poor compressive properties. It may be therefore possible to use the PRD-166 fibres in hybrid composites as a method of improving compressive behaviour. It can also be seen that the fluorescence R_1 line shifts non-linearly with applied strain (Fig. 3(a)). It has been noted elsewhere [13] that a small non-linearity may be present in the R_1 line-shift for stresses less than 3 GPa. However, the reason for this non-linear behaviour is as yet unknown. In contrast, the fluorescence R_2 line (Fig. 3(b)) shows approximately the same linear shift with strain in both tension and compression.

The dependence of the wavenumber of the fluorescence R_2 line upon applied tensile strain was also determined for free-standing fibres with gauge lengths of 20 and 50 mm using the micrometer straining rig. An approximately linear relationship between the wavenumber of the fluorescence R_2 line and tensile strain was also obtained, as has been reported before [8]. It is shown in Fig. 4 that the positive slope (tension) increases with fibre gauge length and extrapolates for an infinite gauge length to the value of slope obtained from the four-point bending test. This behaviour is thought to be due to the end-effects in the micrometer straining rig (i.e the difficulty in defining the gauge length due to the decay of fibre stress in the regions where the fibres are fixed to the aluminium foil tabs with cyanoacrylate adhesive). The longer the gauge length, the less important the end-effects become and thus the larger the expected value of the slope. It should be noted that a lower slope for 20 mm gauge length has been reported earlier for PRD-166 fibres [8]. This may be attributed to a different method of fixing the fibres since a relatively high

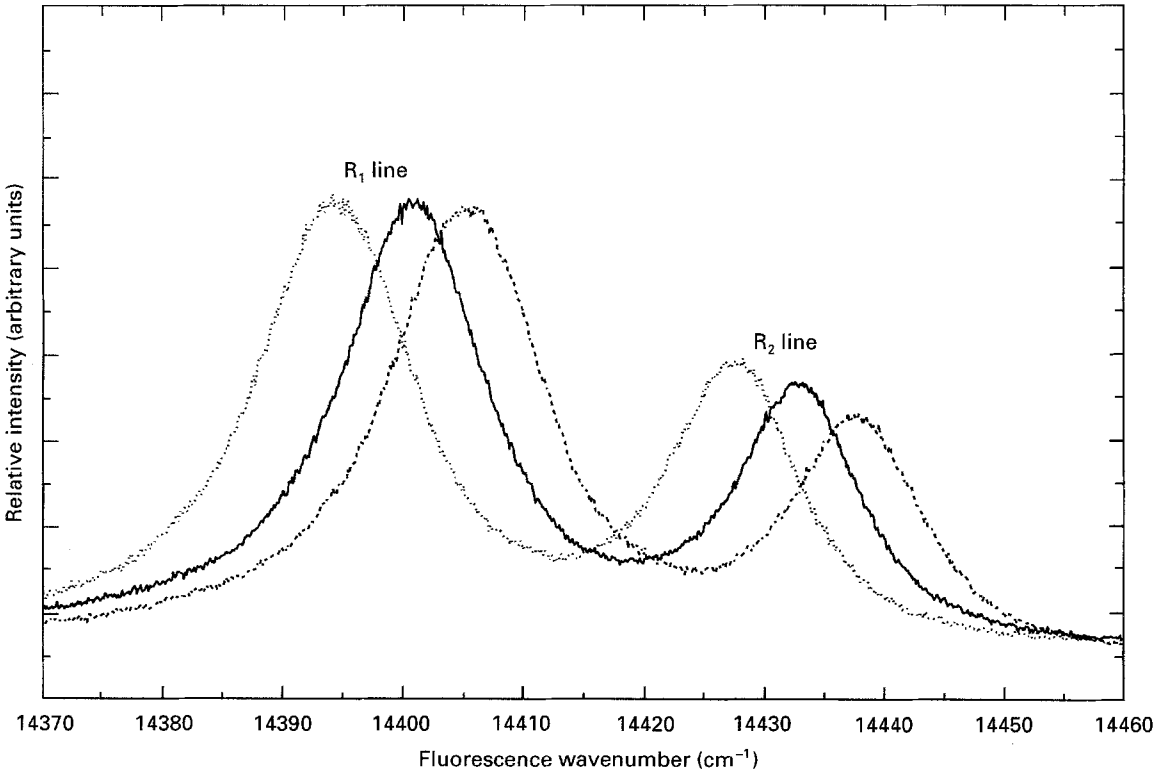

Figure 2 Shift in the positions of the fluorescence R_1 and R_2 lines with applied strain for a PRD-166 fibre. e_{app}: .... − 0.39%; — 0.0%; - - - + 0.44%.

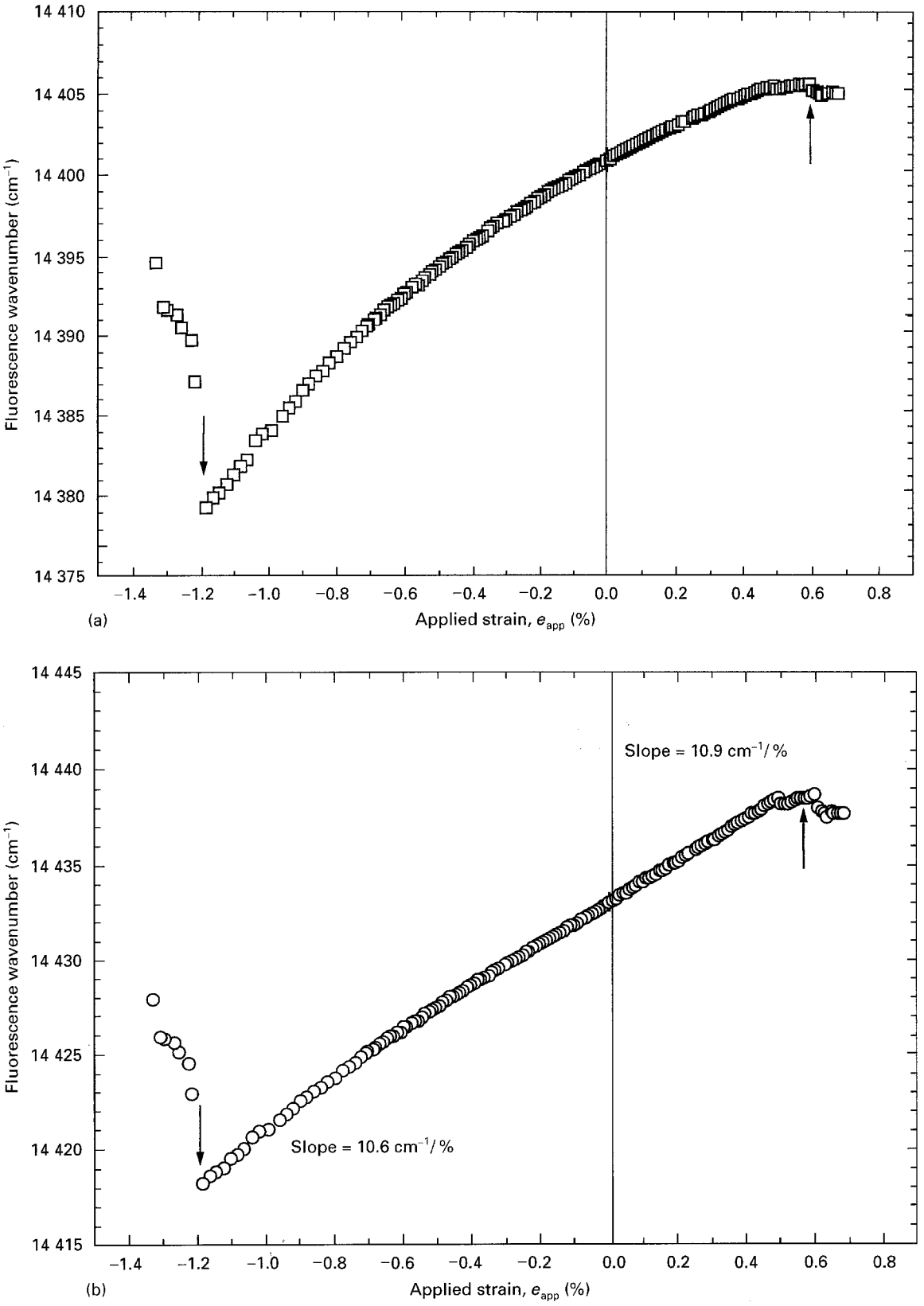

Figure 3 Variation of the wavenumbers of the fluorescence lines with applied strain for a PRD-166 fibre. (Arrows indicate fibre failure). (a) R_1 and (b) R_2 line.

failure strain was also reported in that study. Fig. 4 is a clear demonstration of the advantage of the four-point bending rig for strain calibration.

Because of the difficulties in defining the exact gauge length for the high-modulus PRD-166 fibres it was decided that it would also be of interest to determine the dependence of the peak position of the R_2 line upon fibre stress, since it is not necessary to know the exact gauge length in this case. The R_2 line was chosen because the shift with strain is more linear and the shift rate is higher than for R_1 (Figure 3). The findings are shown in Fig. 5 where it can be seen that the peak shifts approximately linearly to higher wavenumber and the slope of the line is 2.9 cm^{-1} GPa^{-1}. This value can be compared with a value of 2.4 cm^{-1} GPa^{-1} determined for the R_1 line in polycrystalline alumina by Mollis and Clarke [20] and hence is in good agreement since it is known that

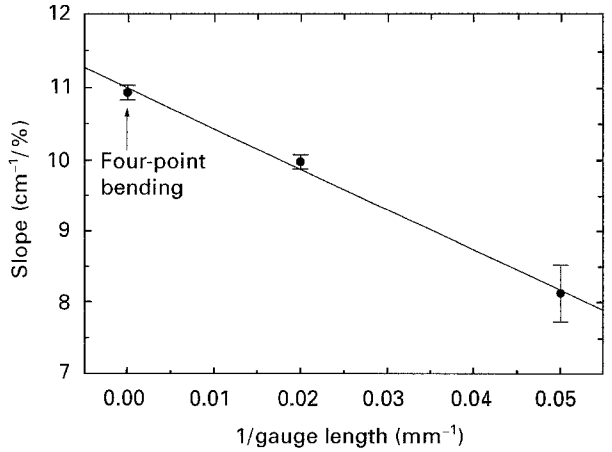

Figure 4 Plot of slope (strain sensitivity of fluorescence R_2 line) versus the reciprocal of the fibre gauge length.

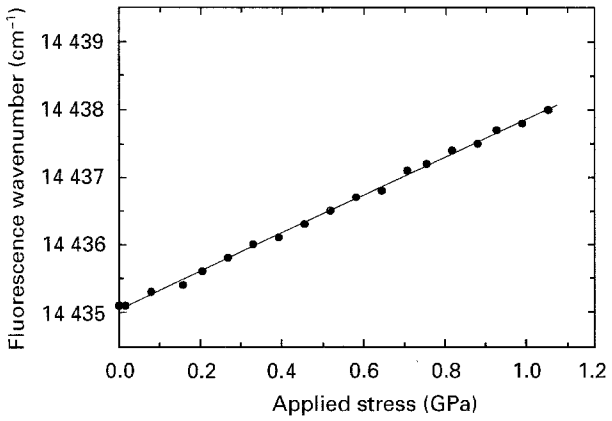

Figure 5 Dependence of the peak position of the fluorescence R_2 line upon applied tensile stress for a PRD-166 fibre deformed in air. Slope = 2.9 cm^{-1} GPa^{-1}

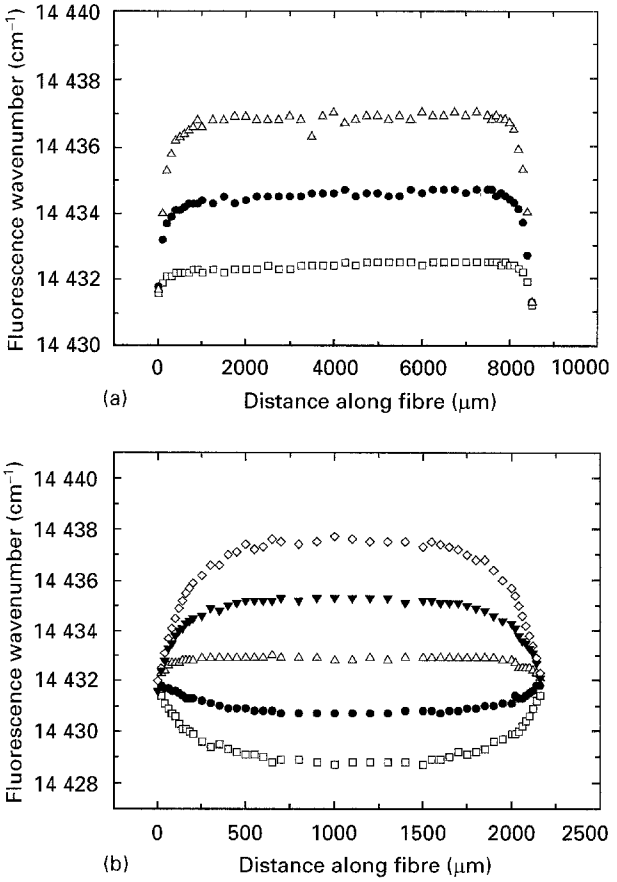

Figure 6 Variation of the wavenumbers of the fluorescence R_2 line with distance along PRD-166 fibres in epoxy matrices, at various levels of applied matrix strain, e_m%. (a) Cold-cured and (b) hot-cured epoxy resin matrix. □ 0.0; ● 0.2; △ 0.4; ▼ 0.6; ◇ 0.8.

the shift rate of the R_2 band a low strain is about 20% higher than that of the R_1 band [20]. The relationship between the R_2 band peak position and stress in Fig. 5 was used to determine fibre stress during deformation in the epoxy resin composites.

The values of the stress and strain dependent fluorescence band shift rates can also be used to estimate the fibre modulus. A strain dependence of 10.9 cm^{-1}/% strain and a stress dependence of 2.9 cm^{-1} GPa^{-1} (both in tension) imply a fibre tensile modulus of about 375 GPa which is similar to that of 380 GPa quoted by Chawla [21] for PRD-166.

3.2. Stress mapping before fibre fragmentation

The variation of the wavenumber of fluorescence R_2 line with distance along a PRD-166 fibre in the cold- and hot-cured epoxy matrix, at various levels of applied matrix strain, e_m, is shown in Fig. 6(a) and (b), respectively. The wavenumber was converted into axial fibre stress using the slope of the line obtained from the stress calibration (see Fig. 5).

The variations of fibre stress with distance along the PRD-166 fibre in the cold- and hot-cured epoxy matrix at various levels of applied matrix strain are shown in Fig. 7(a) and (b) respectively. It can be seen from Fig. 7(a) that at the zero matrix strain there is a small tensile stress of approximately 0.3 GPa in the PRD-166 fibre in the cold-cured epoxy matrix. This is possibly due to fibre pre-stretching during alignment in the mould. In contrast, for the fibre in the hot-cured epoxy matrix (Fig. 7(b)) an initial compressive stress of about 1.1 GPa is obtained. Thus, the application of tensile strain to the composite must first of all overcome the initial compression in the fibre before subjecting it to tension. As the matrix strain is increased, the stress in the fibre increases from the fibre ends to a maximum value along the middle region of the fibre.

The distribution of stress along the fibre, as can be seen from Fig. 7(a) and (b), is similar to that predicted by the conventional shear–lag theory [1, 22]. In fact excellent agreement with shear–lag theory was obtained at low levels of applied matrix strain, since both matrix and fibre are in elastic state [23]. The shear–lag theory assumes that no load is transmitted across the fibre ends and, indeed, negligible load (within experimental error) is transmitted across the PRD-166 fibre ends, as can be seen from Fig. 7(a) and 7(b).

3.3. Interfacial shear stresses

The variation of the interfacial shear stress, τ, with distance along the fibre can be determined from the variation of the fibre stress using the well-known

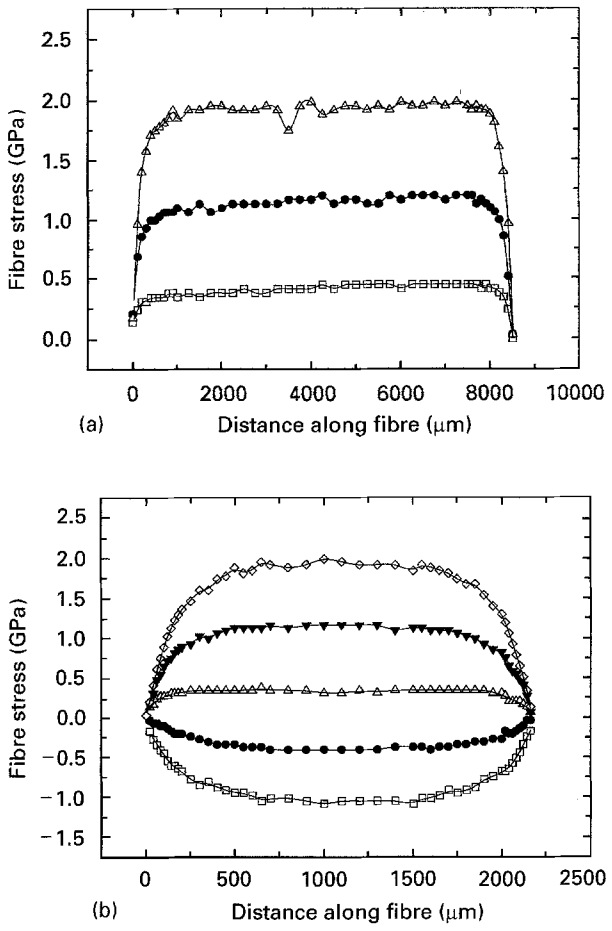

Figure 7 Variation of axial fibre stress with distance along PRD-166 fibres in epoxy matrices, at various levels of applied matrix strain, e_m%. (a) Cold-cured and (b) hot-cured epoxy resin matrix. □ 0.0; ● 0.2; △ 0.4; ▼ 0.6; ◇ 0.8.

force-balance equilibrium [22]

$$\tau = \frac{r}{2}\left(\frac{d\sigma_f}{dx}\right) \quad (1)$$

where r is the fibre radius and $d\sigma_f/dx$ is the differential of the fibre stress with respect to distance along the fibre. The variation of interfacial shear stress with distance along the PRD-166 fibre in the cold- and hot-cured matrix is shown in Fig. 8(a) and (b), respectively. The variation of interfacial shear stress with distance along the fibre was derived by differentiating cubic spline fits of the experimental data in Fig. 7 and substituting $d\sigma_f/dx$ into Equation 1. It can be seen from Fig. 8(a) and (b) that at low levels of matrix strain, the interfacial shear stress is a maximum at the fibre ends and decreases to zero at some distance along the fibre. The variation of interfacial shear stress with distance along the fibre is again similar to that predicted by the shear–lag theory [1, 22].

The variations of the maximum interfacial shear stress, τ_{max}, with applied matrix strain for PRD-166 fibres in the cold- and hot-cured epoxy matrices are shown in Fig. 9(a) and (b), respectively. It can be seen that the maximum interfacial shear stress is approximately proportional to the applied matrix strain, implying that there is no matrix yielding and/or interfacial debonding [7] at these levels of matrix strain. It should be noted that the maximum value of τ_{max} for both the cold- and hot-cured PRD-166/epoxy composites is between 40 and 45 MPa, which is similar to the matrix shear yield stress of about 43 MPa [15, 16]. Hence it appears that the interfacial shear strength, τ_i,

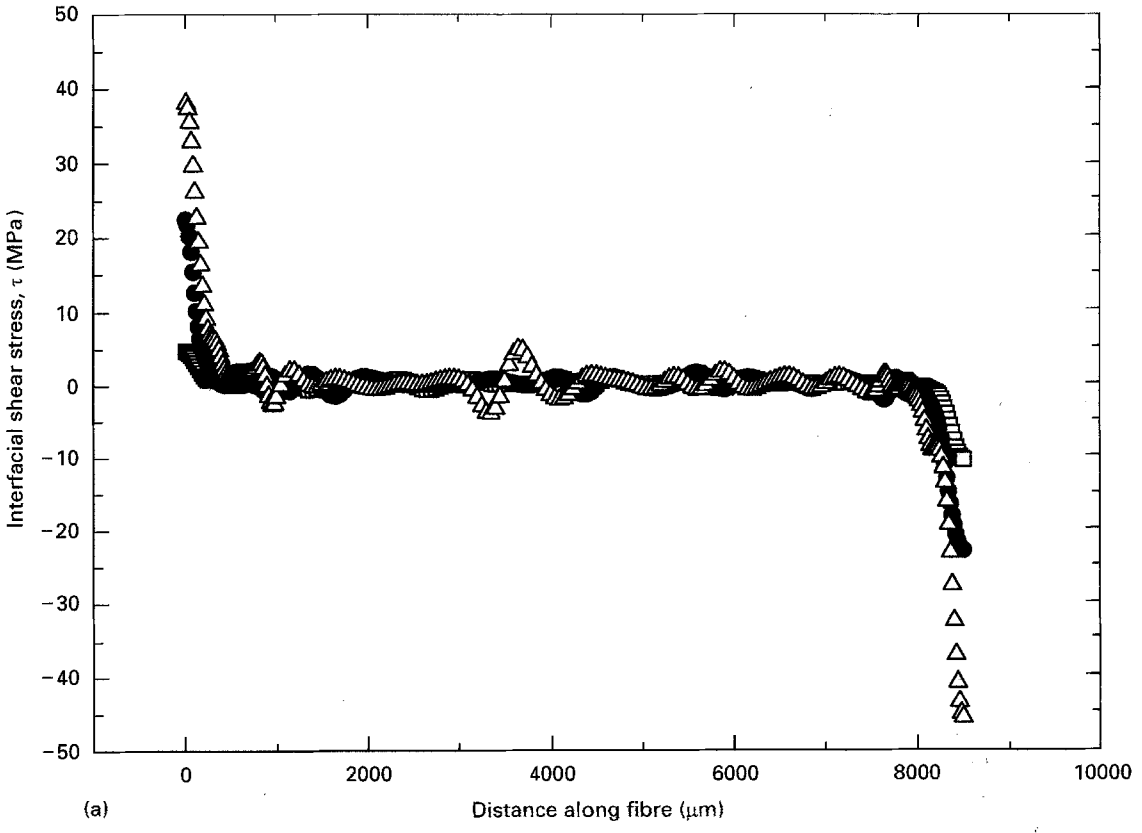

Figure 8 Derived variation of interfacial shear stress, τ, with distance along PRD-166 fibres in epoxy matrices, at various levels of applied matrix strain, e_m%. (a) Cold-cured and (b) hot-cured epoxy resin matrix. □ 0.0; ● 0.2; △ 0.4; ▼ 0.6; ◇ 0.8.

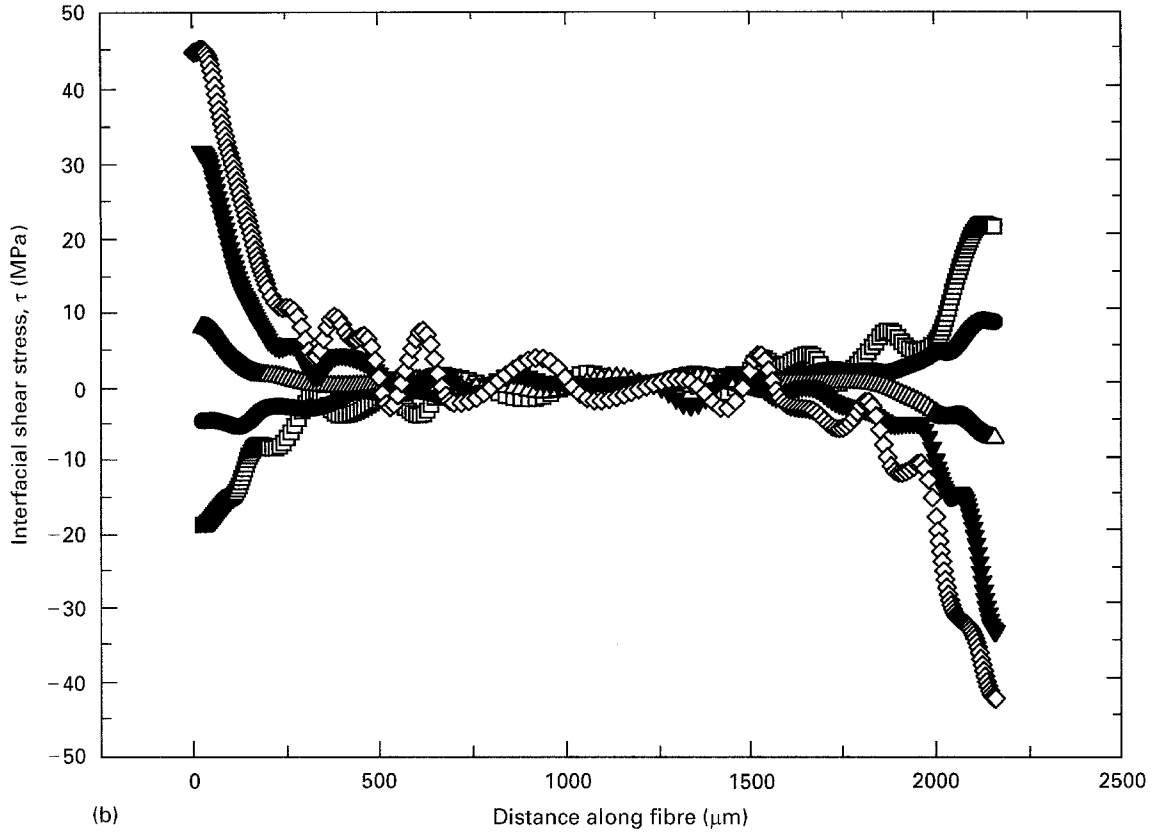

Figure 8 (Continued).

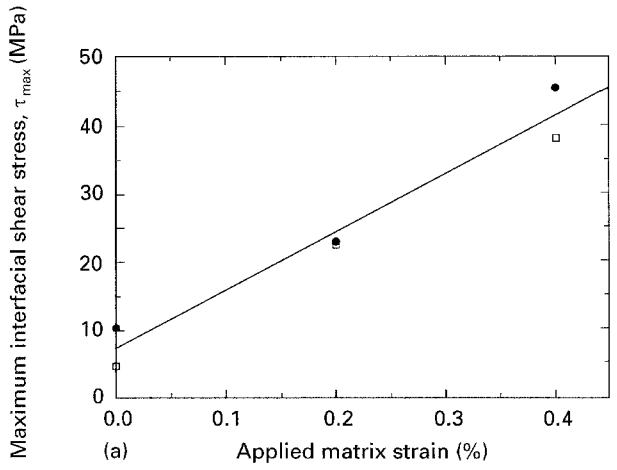

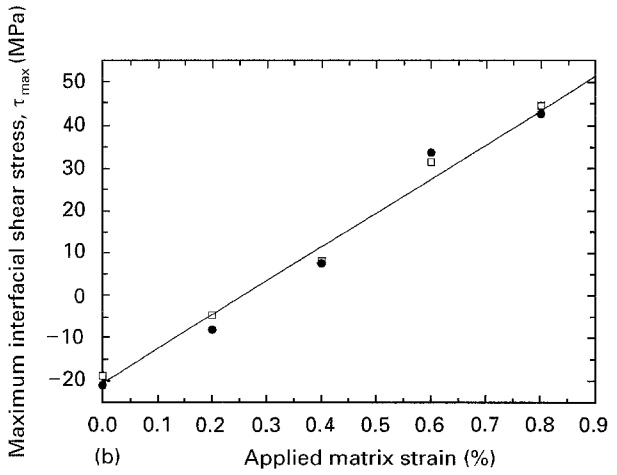

Figure 9 Variation of maximum interfacial shear stress, τ_{max}, with applied matrix strain for a PRD-166 fibre in the (a) cold-cured and (b) hot-cured epoxy resin matrix. □ left end; ● right end.

(the maximum value of τ_{max}) for the PRD-166/epoxy composites studied is controlled by the shear yield strength of the epoxy resin matrix.

3.4. Stress mapping during fibre fragmentation

When a fragmentation test is undertaken upon a single-fibre model composite, a tensile stress is applied to the matrix until the embedded fibre breaks up into a number of fragments [24]. As the stress is increased the fibre fractures repeatedly along its length until all remaining fragments become so short that no further fracture can occur and the specimen is said to have reached the "saturation" state. Fig. 10 shows the distributions of fibre stress with distance along the entire length of a PRD-166 fibre in the hot-cured epoxy matrix. For this sample, the fibre fragmentation was first observed at $e_m = 0.8\%$ (Fig. 10(a)) when the fibre had broken into four fragments. It can be seen that the fibre stress drops to approximately zero at each break point and builds up to reach a maximum in the middle of each fragment. When the matrix strain is increased, the longest fragment breaks approximately at its mid-point, where the stress is highest, and the saturated state is reached at $e_m = 1.2\%$ (Fig. 10(b)). It should be noted that, since a fibre stress of ~ 1.5 GPa corresponds to a strain of less than 0.5% for a fibre with a modulus in excess of 300 GPa, the maximum strain in each fragment is much lower than the matrix strain. Thus, the fibre in the model composite is no longer providing effective reinforcement.

The distributions of fibre stress and interfacial shear stress with distance along Fragment 2 (Fig. 10) at

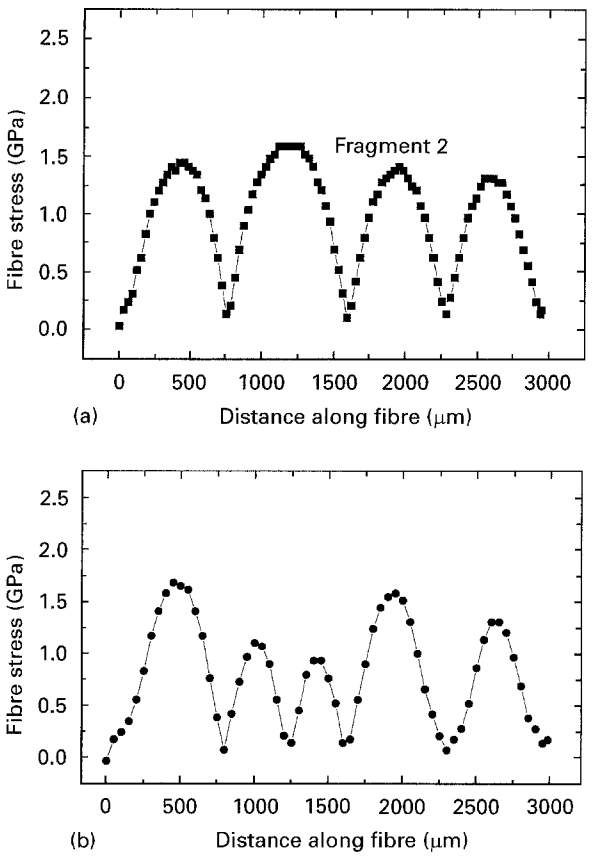

Figure 10 Variation of axial fibre stress along a fragmented PRD-166 fibre in hot-cured epoxy matrix at (a) $e_m = 0.8\%$ and (b) $e_m = 1.2\%$.

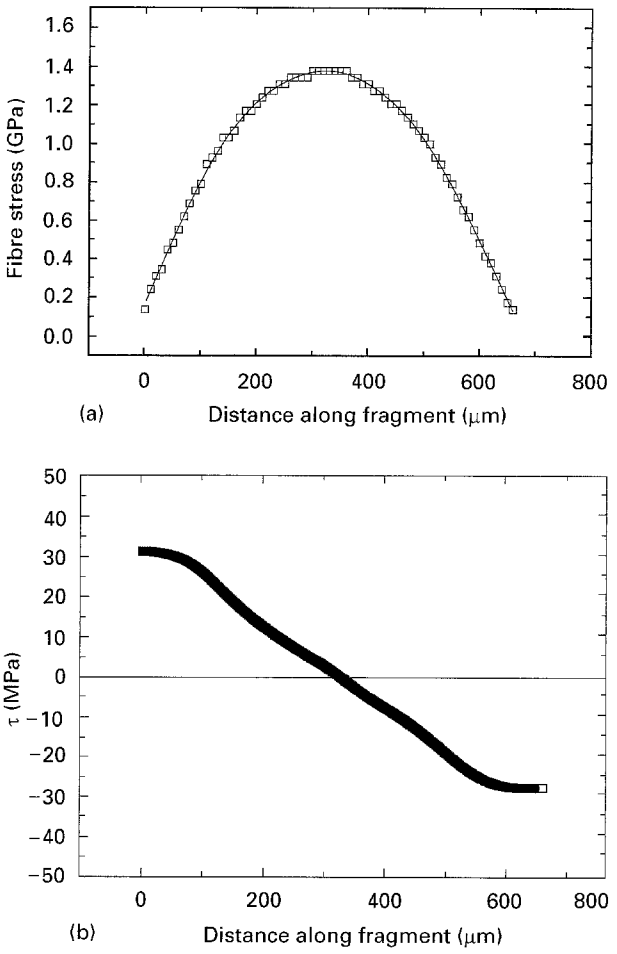

Figure 11 Variation of (a) axial fibre stress and (b) interfacial shear stress along Fragment 2 of the PRD-166 fibre in the hot-cured epoxy matrix at $e_m = 0.8\%$.

various levels of matrix strain are shown in more detail in Figs 11–13. At a matrix strain of 0.8%, just after the onset of fragmentation, the maximum fibre stress (Fig. 11) is in the middle of the fragment and the maximum values of interfacial shear stress occur at the broken ends. These distributions of fibre stress and interfacial shear stress along the fragment are similar to those predicted by the shear-lag model proposed by Cox [1].

It can be seen from Fig. 11(a) that there appears to be good adhesion along the whole length of the fragment and with no evidence of interfacial debonding. This should be contrasted with the fragmentation behaviour of the PRD-166/cold-cured epoxy composite, where significant interfacial debonding is observed at the fibre breaks [23]. This is expected since there is better mechanical interlocking at the fibre/matrix interface in the PRD-166/hot-cured epoxy model composite.

When the matrix strain is increased to 2.0% the form of the stress distribution along the fragment shown in Fig. 12(a) changes markedly due to the interfacial debonding taking place from the fragment ends. This behaviour is also reflected in the distribution of interfacial shear stress shown in Fig. 12(b) where a 150 μm region of constant τ of about 15 MPa is observed at each fragment end. It is clear that debonding has occurred due to the increase in matrix strain. It should be noted that there is perfect adhesion in the central part of the fragment and the maximum interfacial shear stress is about 40 MPa, which is just below the shear yield stress of the resin.

As the matrix strain is increased further to 3.0%, the interfacial debonded region propagates further along the fragment to over 200 μm from the fibre breaks (Fig. 13). It can be seen that the distributions of axial fibre stress and interfacial shear stress along the fragment shown in Figs 12 and 13 are similar to those predicted using the partial debonding model proposed by Piggott [2].

It might be expected that debonding could occur over the entire fragment length at high levels of matrix strain. The distributions of axial fibre stress and interfacial shear stress along the totally debonded fragment would then be similar to those predicted by the Kelly–Tyson model [3] for a yielding interface. Such behaviour was not found, and there always appeared to be a bonded region along the central region of the fibre, although it is not possible to be absolutely certain since matrix fracture occurs before complete interfacial bebonding of the fragment is obtained. If the fragment were debonded completely from each end, however, there would be a singularity due to a step change in interfacial shear stress in the middle of the fibre that cannot occur in practice [25].

3.5. Residual thermal stresses

An initial compressive stress of about 1.1 GPa was measured in the middle of the PRD-166 fibres in the

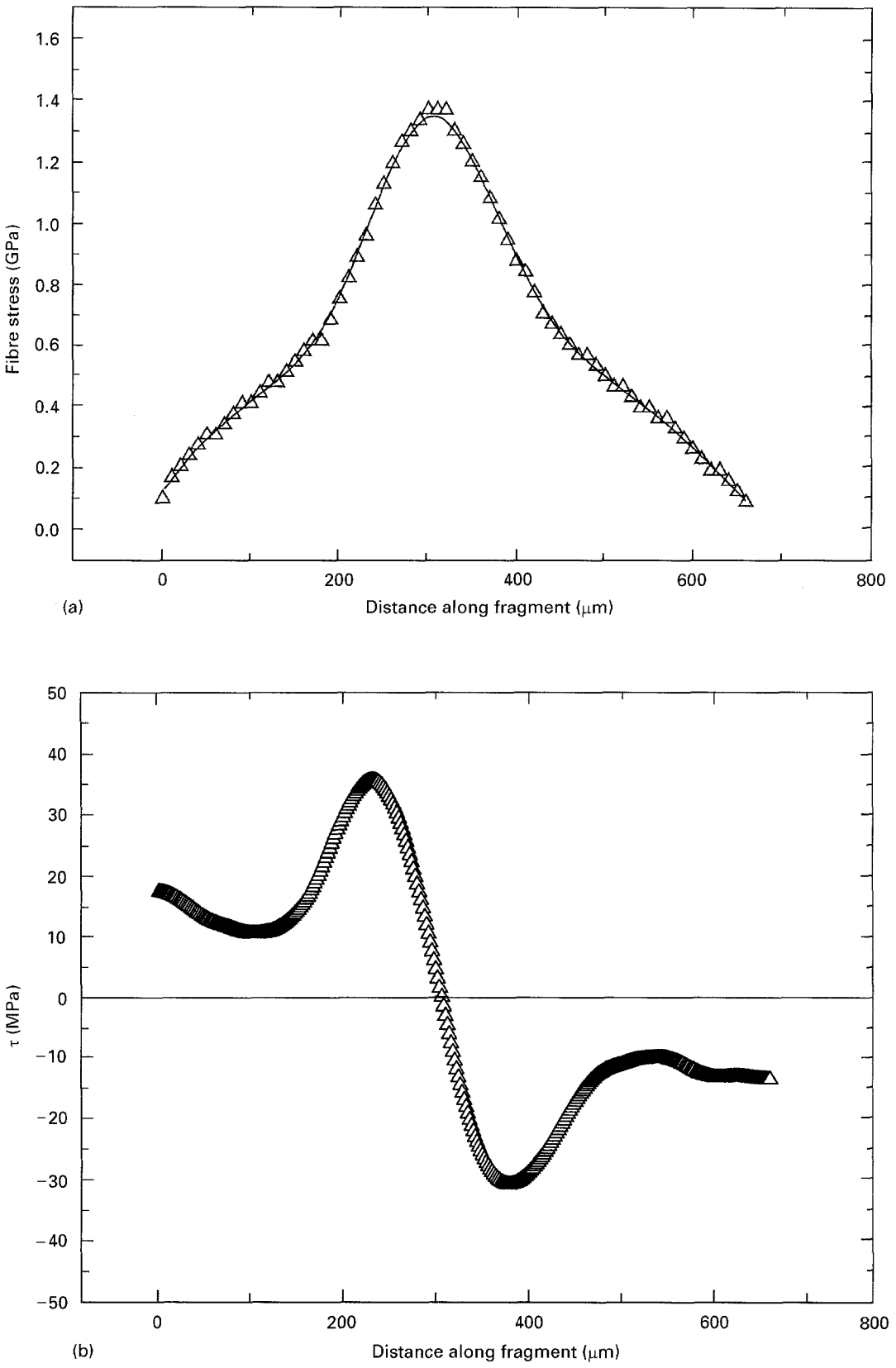

Figure 12 Variation of (a) axial fibre stress and (b) interfacial shear stress along Fragment 2 of the PRD-166 fibre in the hot-cured epoxy matrix at $e_m = 2.0\%$.

hot-cured epoxy matrix (see Fig. 7(b)). This residual stress is expected to develop during cooling of the composite from the processing temperature due to a mismatch of thermal expansion coefficients between the matrix and fibre [21]. It corresponds to an axial fibre strain of about 0.3%. The thermal expansion coefficient of alumina fibre, α_f, is about $8 \times 10^{-6}\,K^{-1}$ [26] and that of epoxy matrix, α_m, is about $60 \times 10^{-6}\,K^{-1}$ [27]. Thus on cooling, the greater shrinkage of the epoxy matrix causes axial compression of the fibre. Large residual thermal strains have also been found in PRD-166 fibre embedded in glass matrix [8].

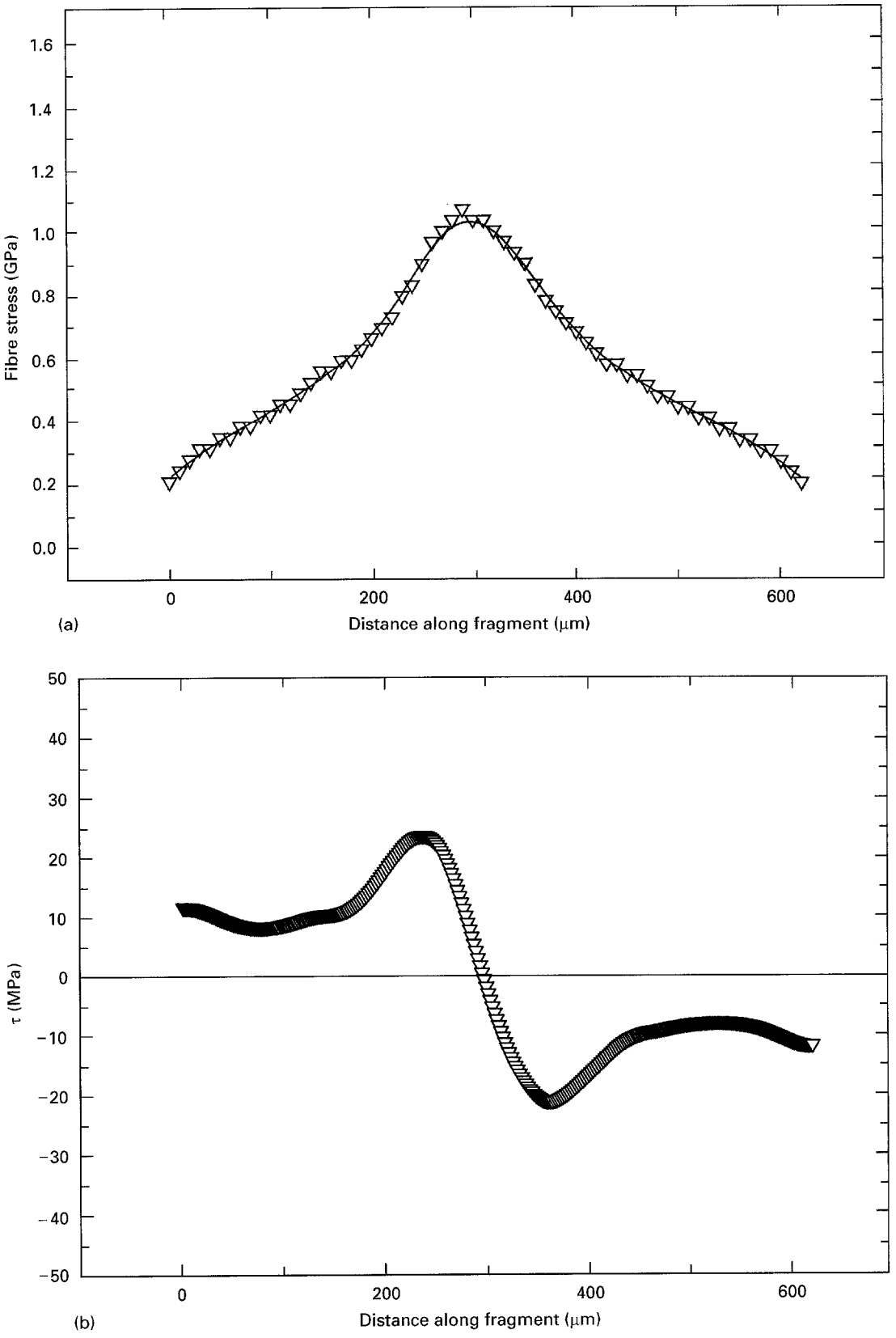

Figure 13 Variation of (a) axial fibre stress and (b) interfacial shear stress along Fragment 2 of the PRD-166 fibre in the hot-cured epoxy matrix at $e_m = 3.0\%$.

The equation for the lower bound of residual strain developed from Nairn's analysis for polymer-based composite [28] can be used to calculate the residual thermal strain in single-fibre composites. Taking the fibre volume fraction, $V_f = 0$, the matrix volume fraction, $V_m = 1$, and the upper temperature limit as the curing temperature, T, Nairn's analysis gives a value of axial strain in the fibre of

$$e_{fz} = \int_{T_0}^{T} \Delta\alpha \mathrm{d}T \tag{2}$$

where $\Delta\alpha = \alpha_f - \alpha_m$, $T = 80\,^{\circ}\mathrm{C}$ and $T_0 = 25\,^{\circ}\mathrm{C}$. Equation 2 predicts a value of 0.29% which corresponds

to the experimental value determined using the shift of the fluorescence R_2 line.

4. Conclusions

It has been demonstrated that well-defined fluorescence band shifts are obtained when PRD-166 alumina-zirconia fibres are subjects to axial deformation. The bands are found to shift to higher wavenumber in tension and to lower wavenumber in compression. Accurate calibrations have been obtained for the dependencies of the band positions both upon tensile and compressive strain and upon tensile stress.

It has been demonstrated that fluorescence spectroscopy is also an excellent technique for following the deformation of the fibres in model epoxy–matrix composites. The distributions of axial fibre stress along a PRD-166 fragment have been determined prior to, during and after saturation of the fibre fragmentation process. The distributions of axial fibre stress along a PRD-166 fibre in a hot-cured epoxy matrix have been determined in detail and are found to be in agreement with those predicted by shear–lag theory following initial fragmentation. The interfacial shear stress distribution along the fibre has been derived from the force–balance argument and the behaviour is similar to that predicted by shear–lag theory. Debonding of the fibre/matrix interface was found to occur from the fragment ends as the matrix strain was increased further and it was found that the debonded regions propagated along the fragment with increasing matrix strain. The behaviour was compared qualitatively with the various load transfer models that can be used to describe fibre stress distributions during fragmentation. This will be the subject of more detailed analysis in a subsequent publication [23].

Acknowledgements

The authors are grateful to E. I. Du Pont de Nemours for supplying the PRD-166 fibres used in this study. One of the authors (RJY) is grateful to the Royal Society for support in the form of the Wolfson Professorship in Materials Science.

References

1. H. L. COX, *Brit. J. Appl. Phys.* **3** (1952) 72.
2. M. R. PIGGOTT, *Compos. Sci. Technol.* **42** (1991) 57.
3. A. KELLY and W. R. TYSON, *J. Mech. Phys. Solids* **13** (1965) 329.
4. C. GALIOTIS, R. J. YOUNG, P. H. J. YEUNG and D. N. BATCHELDER, *J. Mater. Sci.* **19** (1984) 3640.
5. H. JAHANKHANI and C. GALIOTIS, *J. Compos. Mater.* **25** (1991) 609.
6. N. MELANITIS, C. GALIOTIS, P. L. TETLOW and C. K. L. DAVIES, *Ibid.* **26** (1992) 574.
7. M. C. ANDREWS, R. J. DAY, X. HU and R. J. YOUNG, *Compos. Sci. Technol.* **48** (1993) 255.
8. X. YANG and R. J. YOUNG, *Acta Metall. Mater.* **43** (1995) 2407.
9. A. L. SCHAWLOW, in "Advances in quantum electronics", edited by J. R. Singer (Columbia University Press, New York, 1961) p. 50.
10. E. FEHER and M. D. STURGE, *Phys. Rev.* **172** (1968) 244.
11. S. E. MOLLIS and D. R. CLARKE, *J. Amer. Ceram. Soc.* **73** (1990) 3189.
12. Q. MA and D. R. CLARKE, *Acta Metall. Mater.* **41** (1993) 1817.
13. H. HOUGH, J. DEMAS, T. O. WILLIAMS and H. N. G. WADLEY, *Ibid.* **43** (1995) 821.
14. X. YANG, X. HU, R. J. DAY and R. J. YOUNG, *J. Mater. Sci.* **27** (1992) 1409.
15. M. C. ANDREWS and R. J. YOUNG, *J. Raman Spectrosc.* **24** (1993) 539.
16. M. C. ANDREWS, Ph.D. Thesis, Victoria University of Manchester, 1995.
17. Q. MA and D. R. CLARKE, Experiments in smart materials and structures, AMD-Vol. 181 (edited by K.-S. Kim) Book No. H00888, p. 27 (1993).
18. M. C. ANDREWS and R. J. YOUNG, *Polymer*, in press.
19. N. MELANITIS and C. GALIOTIS, *J. Mater. Sci.* **25** (1990) 5081.
20. S. E. MOLLIS and D. R. CLARKE, *J. Amer. Ceram. Soc.* **73** (1990) 3189.
21. K. K. CHAWLA, "Ceramic matrix composites" (Chapman & Hall, London, 1993).
22. A. KELLY and N. H. MACMILLAN, "Strong solids", 2nd Edn. (Oxford University Press, Oxford, 1973).
23. R. B. YALLEE and R. J. YOUNG, to be published.
24. Y. HUANG and R. J. YOUNG, *Comp. Sci. Tech.* **52** (1994) 505.
25. L. N. McCARTNEY, Private communication.
26. A. R. BUNSELL, "Ceramic–matrix composites", edited by R. Warren (Chapman & Hall, New York, 1992), p. 14.
27. D. HULL, "An introduction to composite materials" (Cambridge Solid State Science Series, Cambridge, 1981).
28. J. A. NAIRN, *Mechanics of Materials* **13** (1992) 13.

Received 3 January
and accepted 15 January 1996